Synthesis, coordination chemistry and photophysical properties of naphtho-fused pyrazole ligands

Supporting Information

Rohan J. Weekes[a] and Chris S. Hawes*[a]

[a]School of Chemical and Physical Sciences, Keele University, Keele ST5 5BG, U.K.

Email: c.s.hawes@keele.ac.uk

Contents:

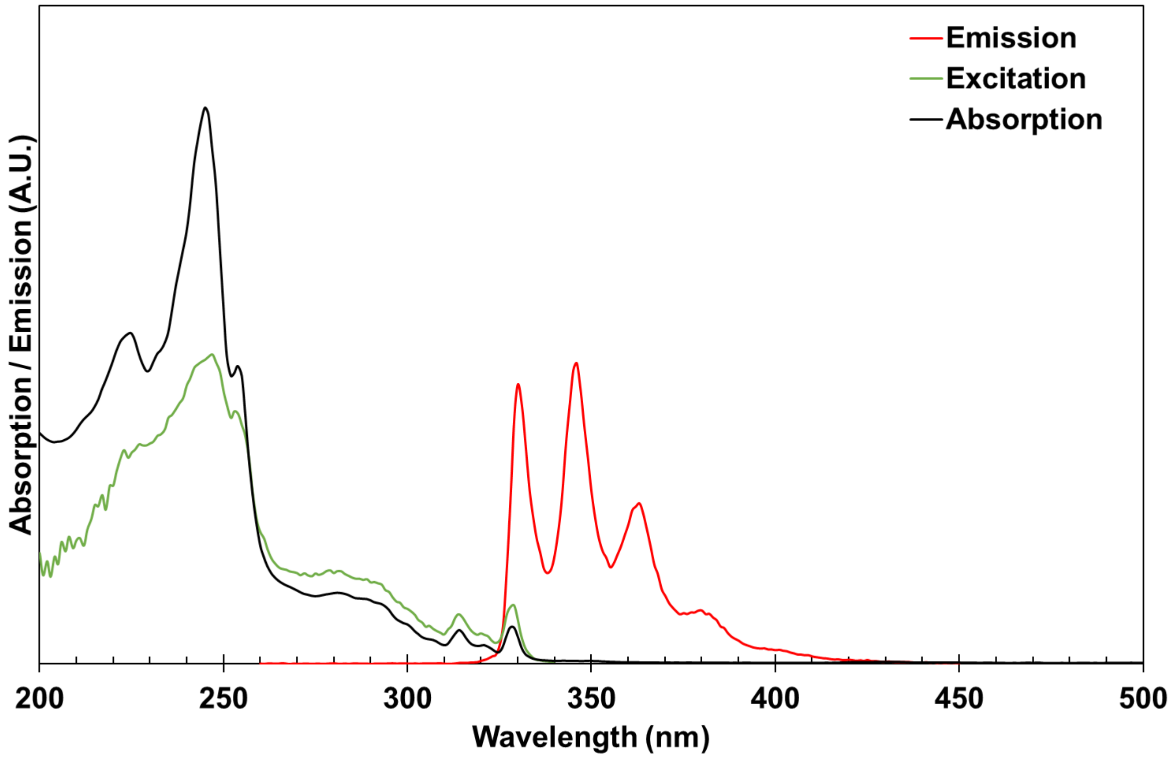

Figure S1 Absorption, emission (λ_{ex} = 245 nm) and excitation (λ_{em} = 345 nm) for **HL1** in MeCN (17 μM).

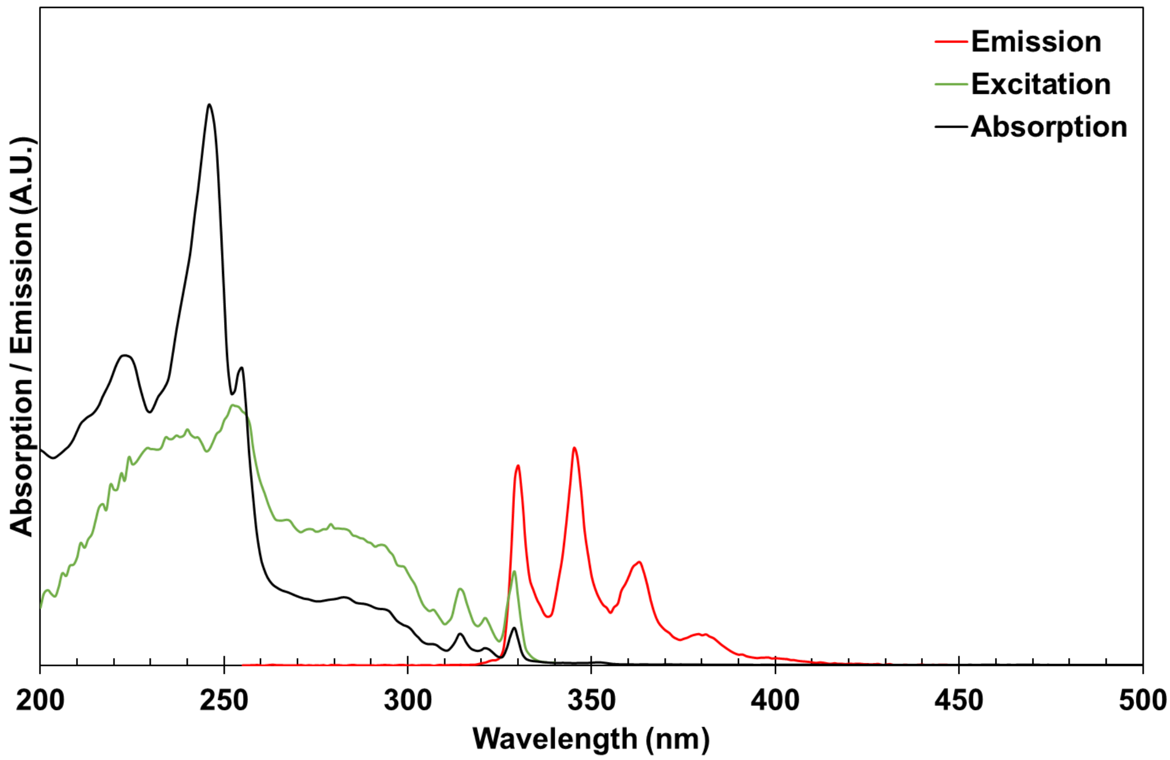

Figure S2 Absorption, emission (λ_{ex} = 245 nm) and excitation (λ_{em} = 345 nm) for **HL1** in hexane (35 μM).

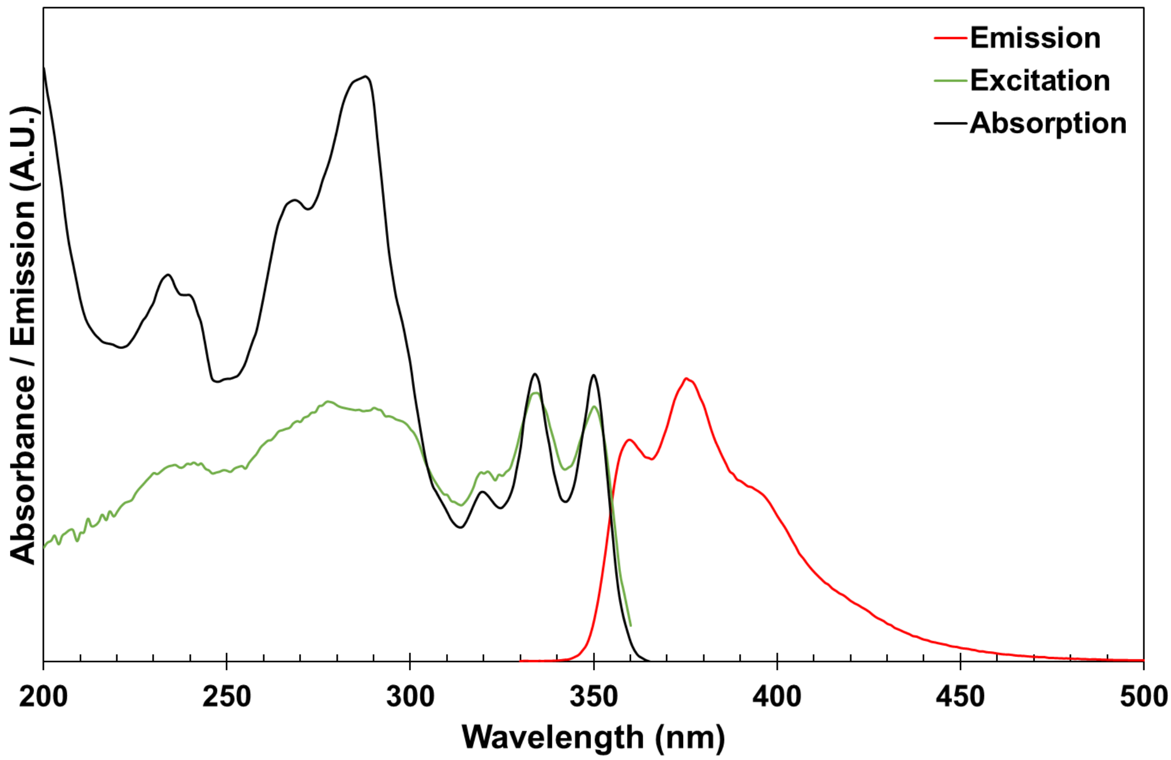

Figure S3 Absorption, emission (λ_{ex} = 320 nm) and excitation (λ_{em} = 373 nm) for **L2** in MeCN (30 μM).

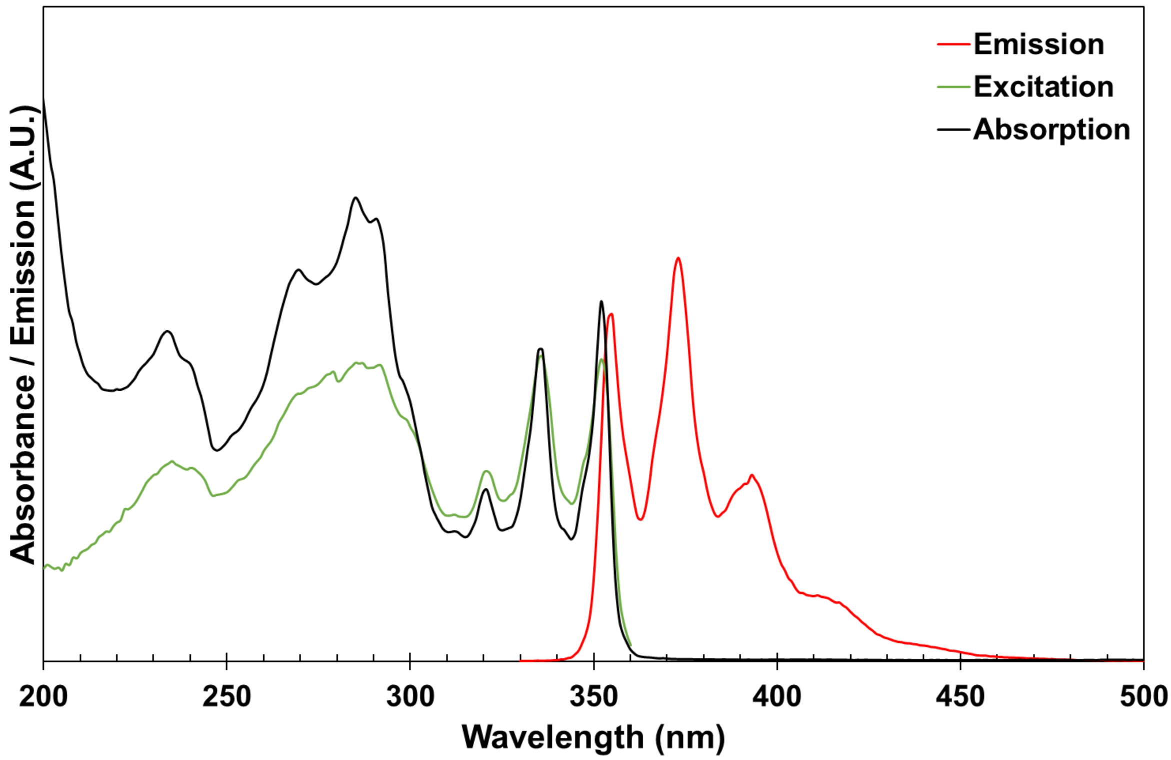

Figure S4 Absorption, emission (λ_{ex} = 320 nm) and excitation (λ_{em} = 373 nm) for **L2** in hexane (15 μM).

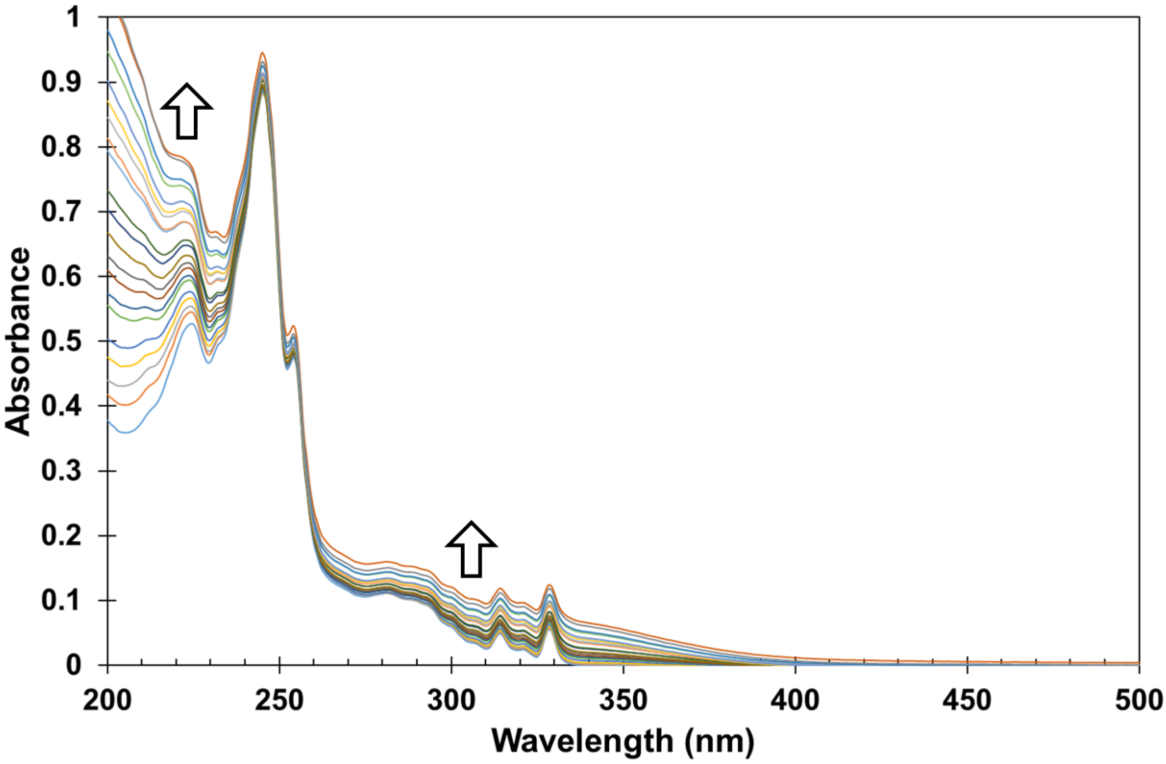

Figure S5 Absorption spectra for **HL1** following sequential additions of $Cu(NO_3)_2 \cdot 2.5H_2O$ at 23 μM concentration in acetonitrile, up to a maximum of 1.4 equivalents.

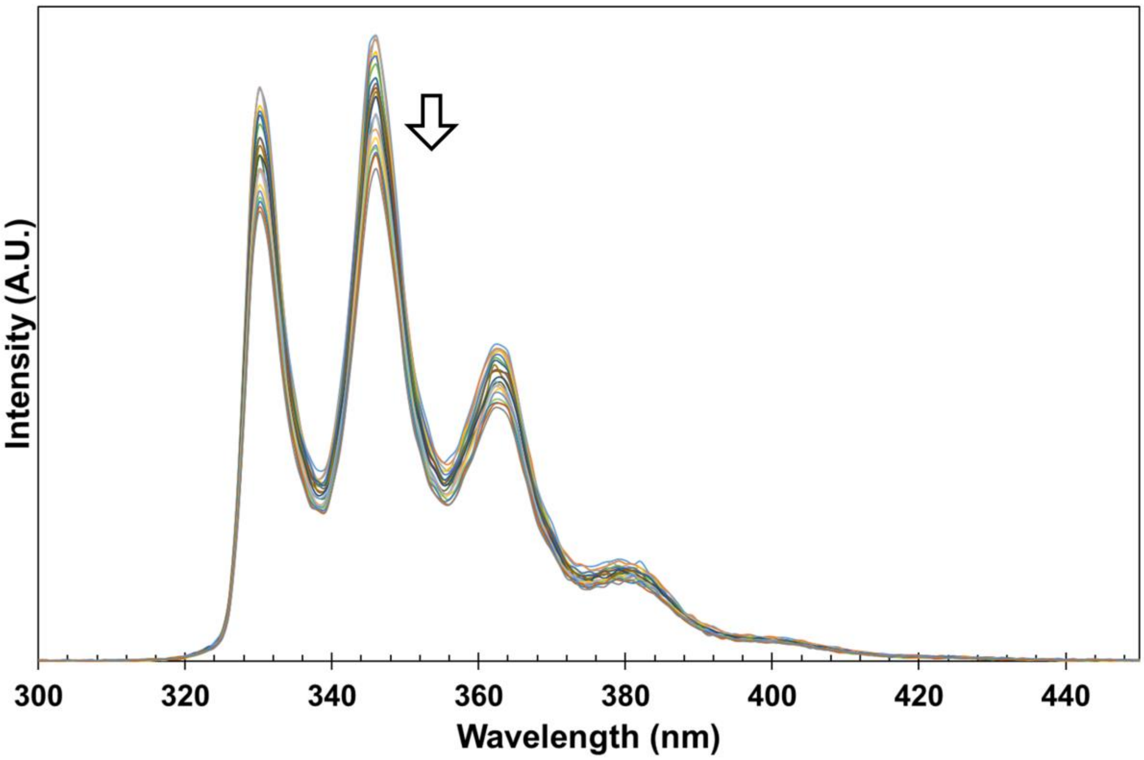

Figure S6 Emission spectra (λ_{ex} = 245 nm) for **HL1** following sequential additions of $Cu(NO_3)_2 \cdot 2.5H_2O$ at 23 μM concentration in acetonitrile, up to a maximum of 1.4 equivalents.

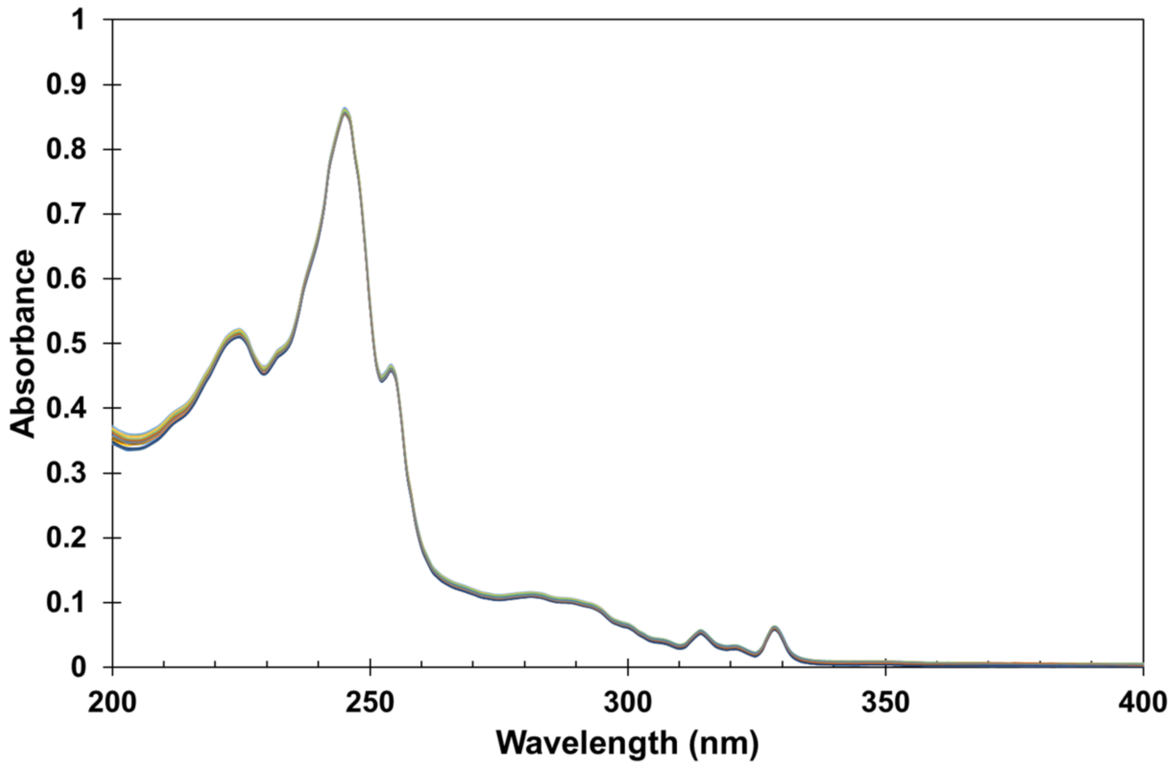

Figure S7 Absorption spectra for **HL1** following sequential additions of $ZnCl_2$ at 23 μM concentration in acetonitrile up to a maximum of 1.6 equivalents.

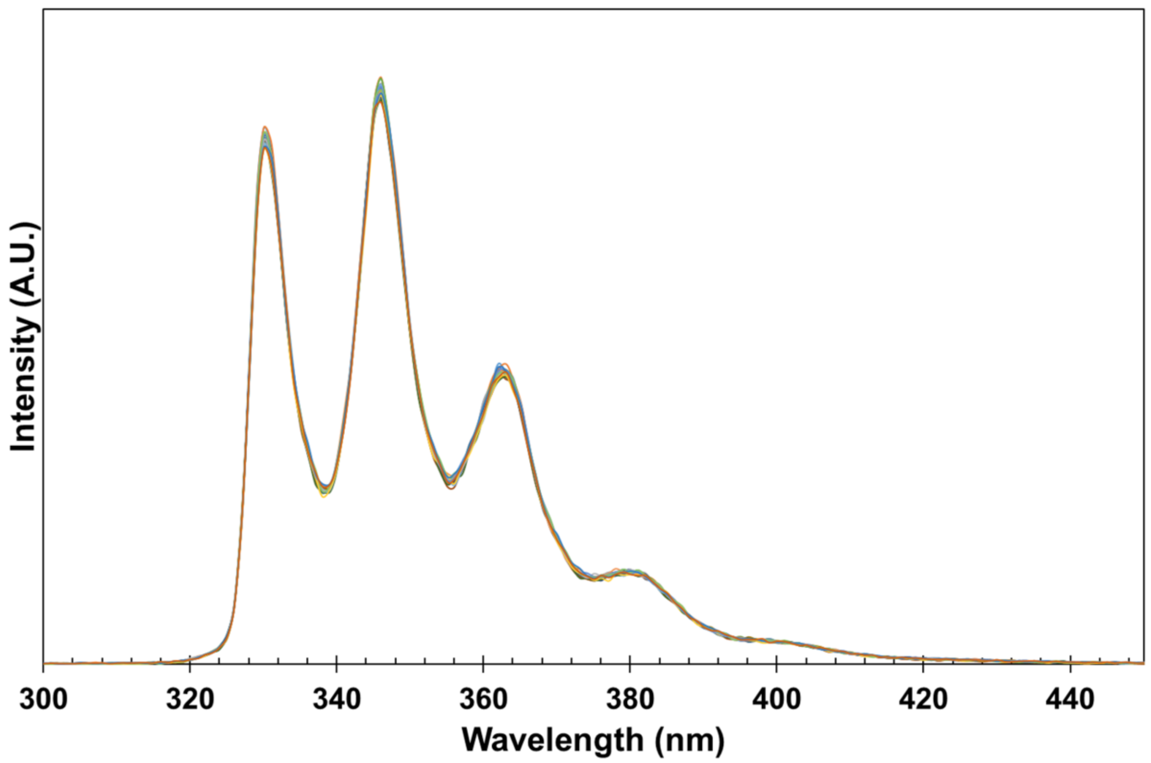

Figure S8 Emission spectra (λ_{ex} = 245 nm) for **HL1** following sequential additions of $ZnCl_2$ at 23 μM concentration in acetonitrile up to a maximum of 1.6 equivalents.

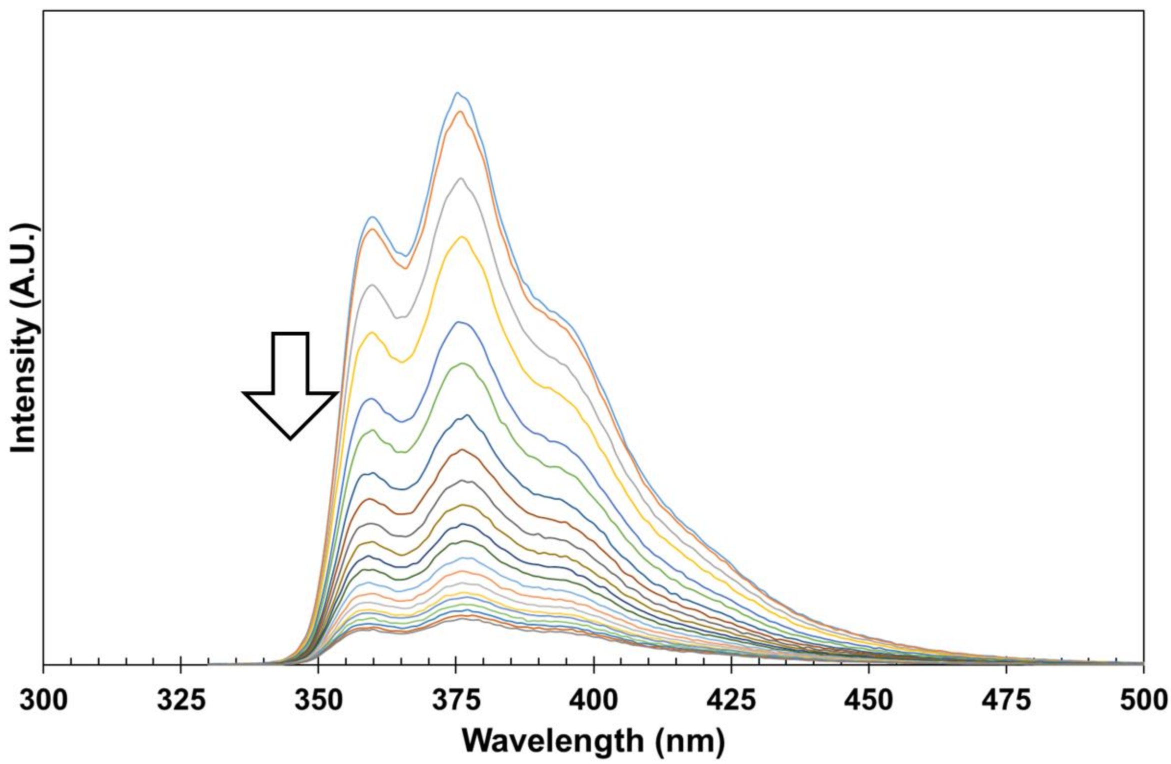

Figure S9 Emission spectra (λ_{ex} = 320 nm) for **L2** at 30µM following sequential additions of $Cu(NO_3)_2 \cdot 2.5H_2O$ up to a maximum of 1.4 equivalents.

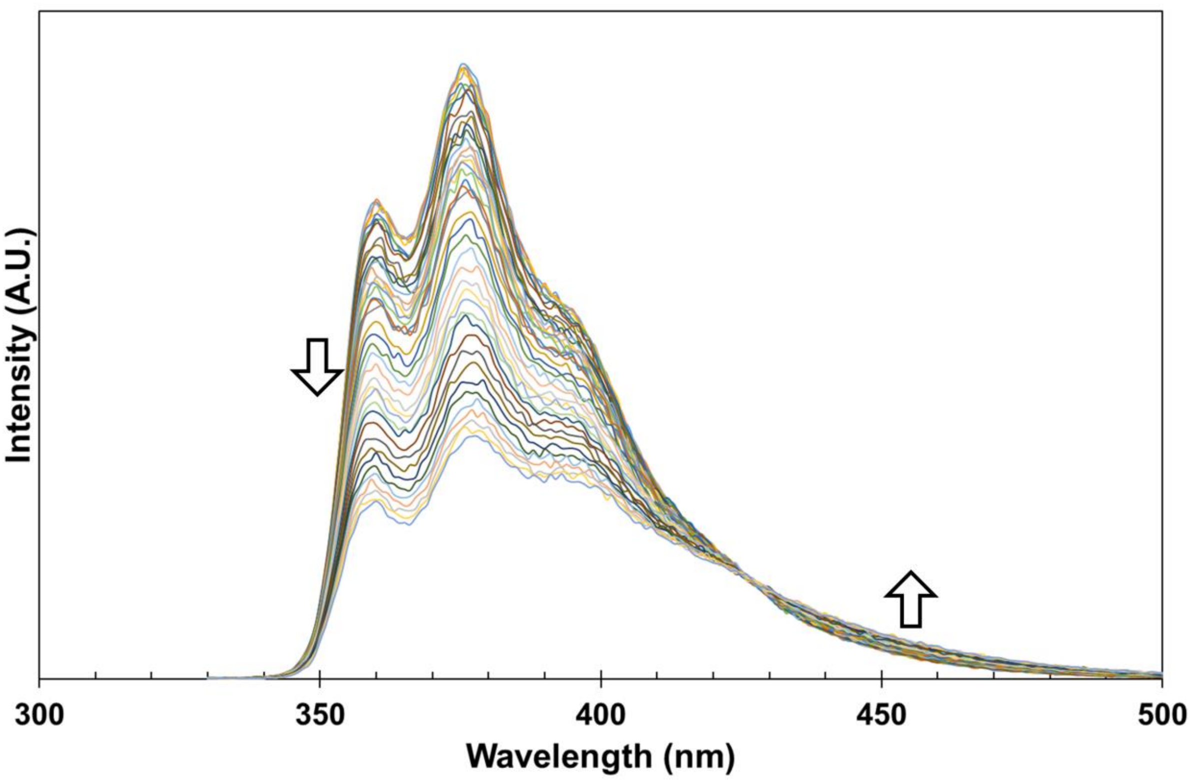

Figure S10 Emission spectra (λ_{ex} = 320 nm) for **L2** at 30µM following sequential additions of $ZnCl_2$ up to a maximum of 12 equivalents.

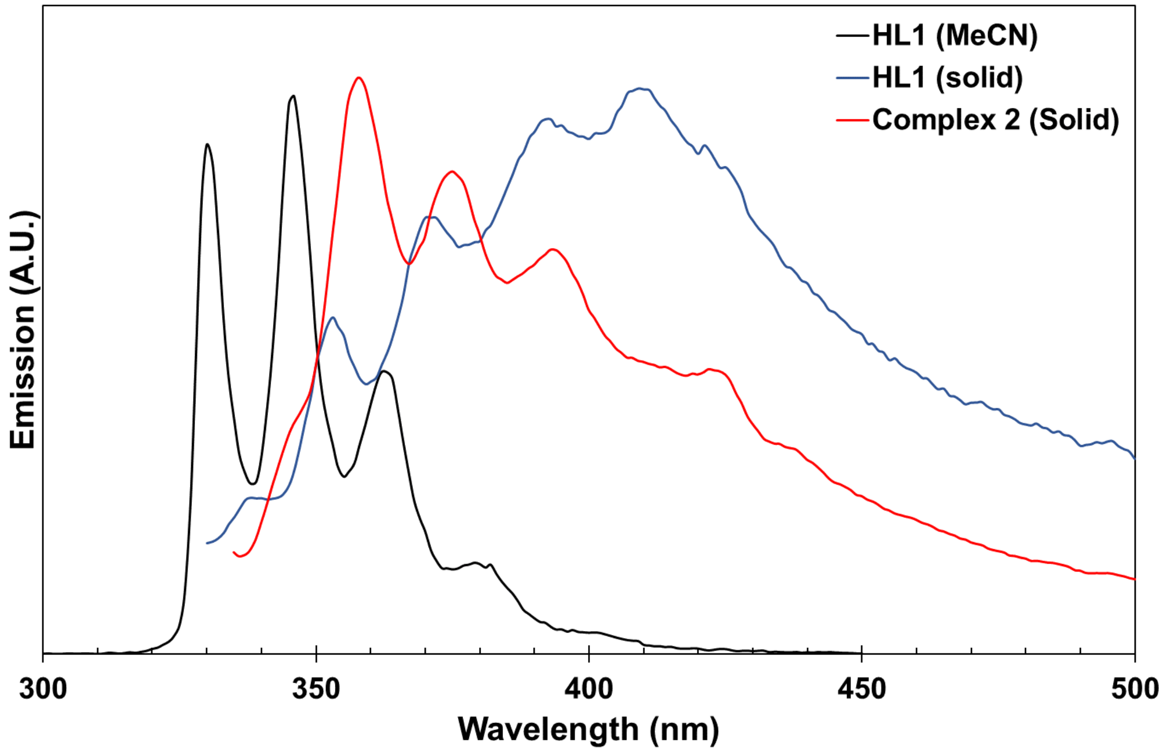

Figure S11 Overlaid emission spectra for **HL1** in solution (MeCN 17 μM, λ_{ex} = 245 nm, black), solid **HL1** (blue, λ_{ex} = 300 nm), and solid complex **2** (red, λ_{ex} = 320 nm)

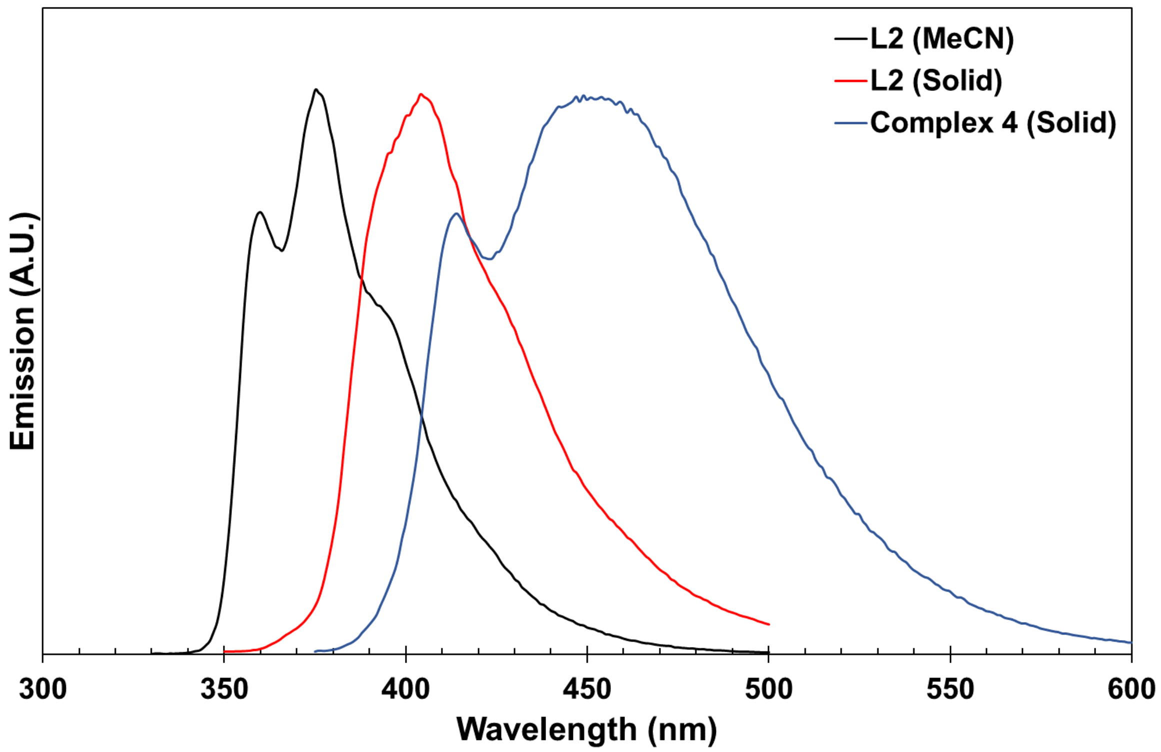

Figure S12 Overlaid emission spectra for **L2** in solution (MeCN 30 μM, λ_{ex} = 320 nm, black), solid **L2** (red, λ_{ex} = 300 nm), and solid complex **4** (red, λ_{ex} = 320 nm)

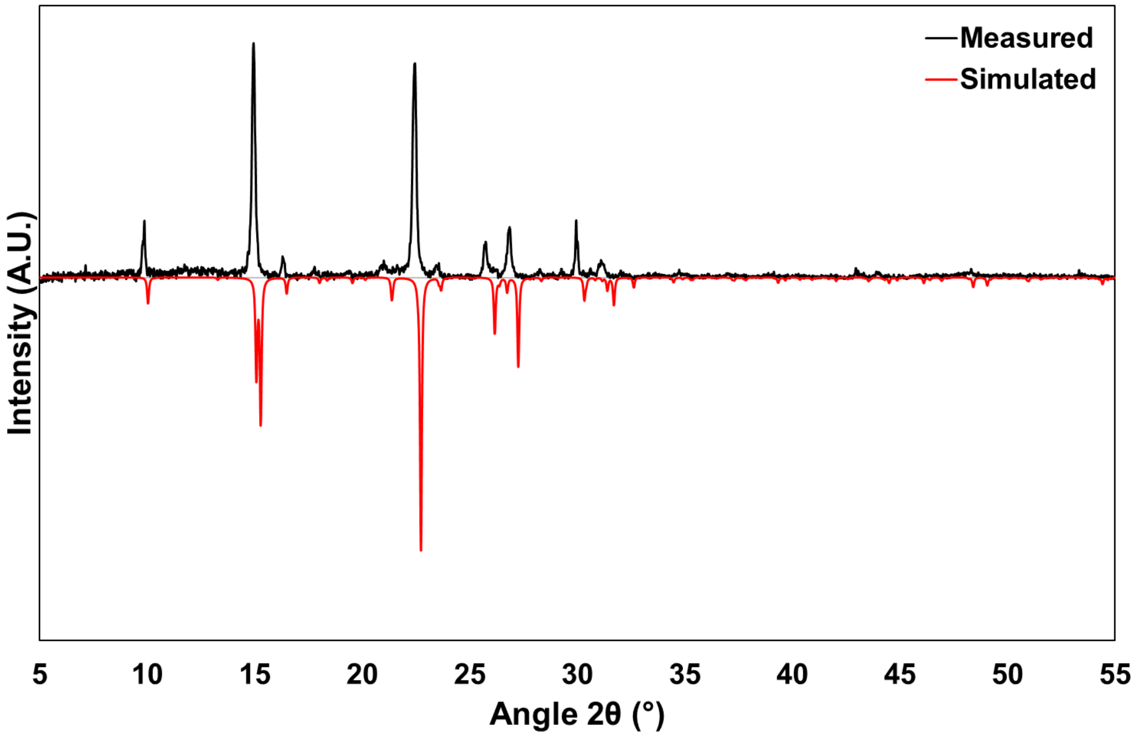

Figure S13 X-ray powder diffraction pattern for **HL1**, showing measured data (black, room temperature) and pattern simulated from single crystal data at 150 K (red)

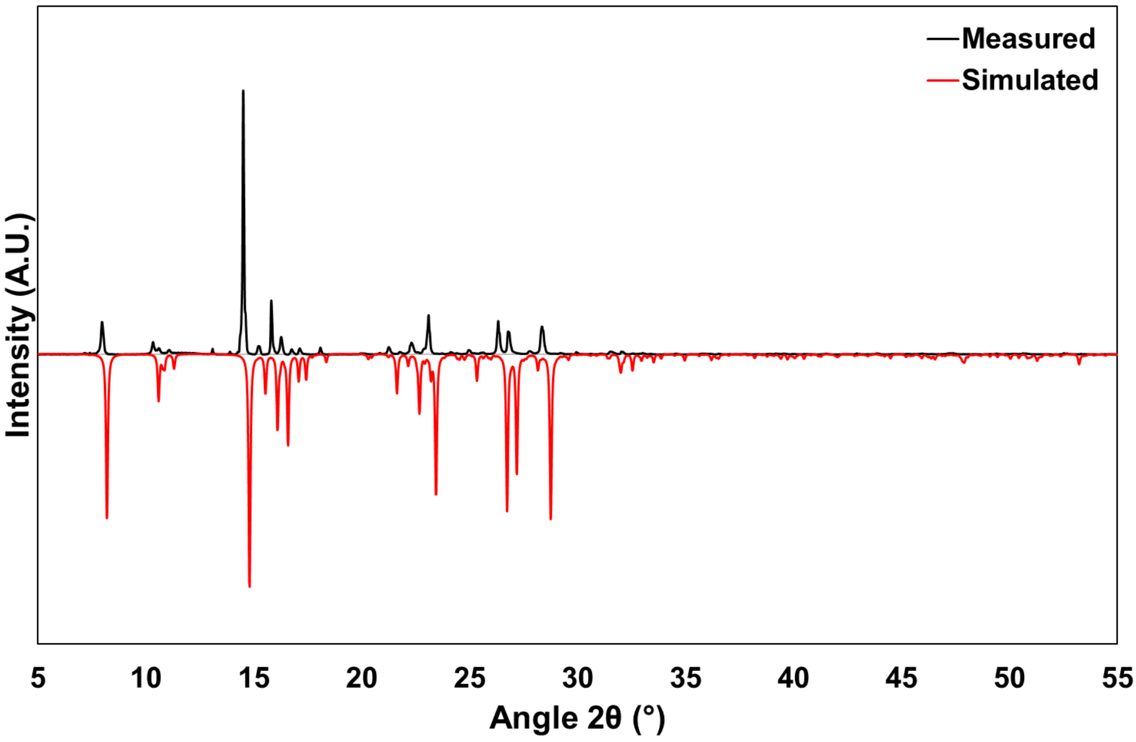

Figure S14 X-ray powder diffraction pattern for **L2**, showing measured data (black, room temperature) and pattern simulated from single crystal data at 150 K (red)

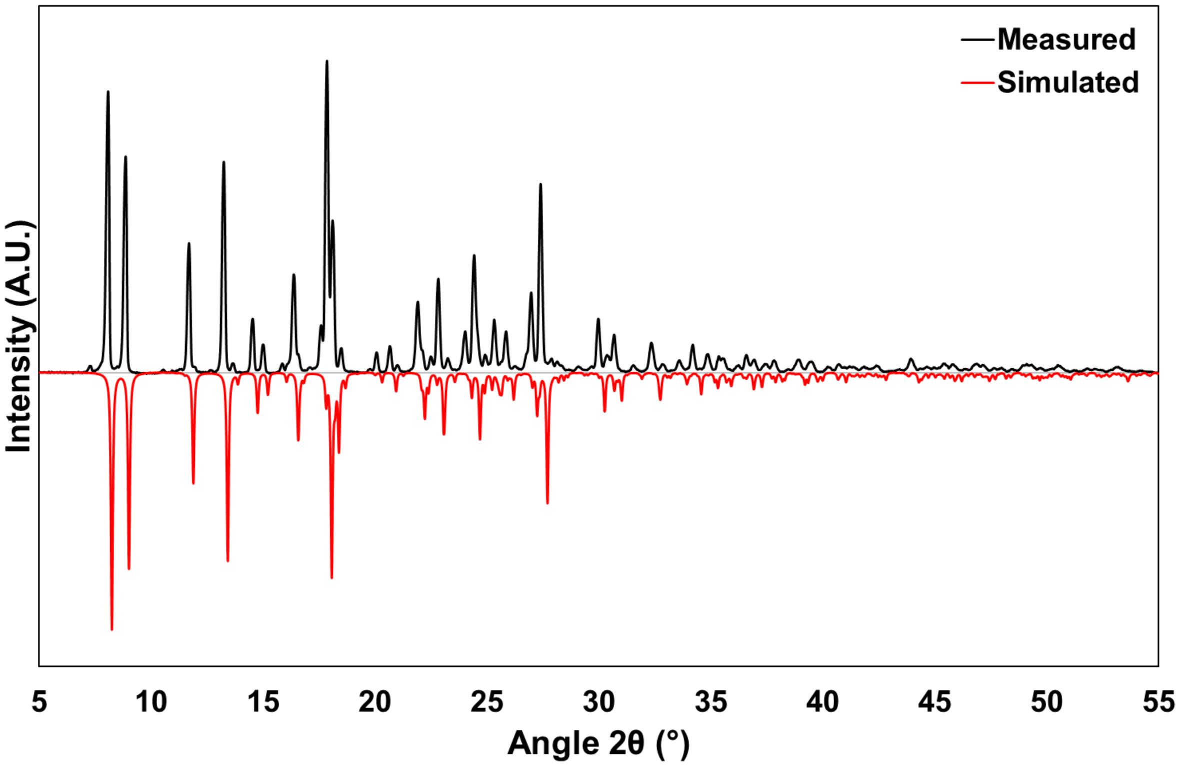

Figure S15 X-ray powder diffraction pattern for complex **1**, showing measured data (black, room temperature) and pattern simulated from single crystal data at 150 K (red)

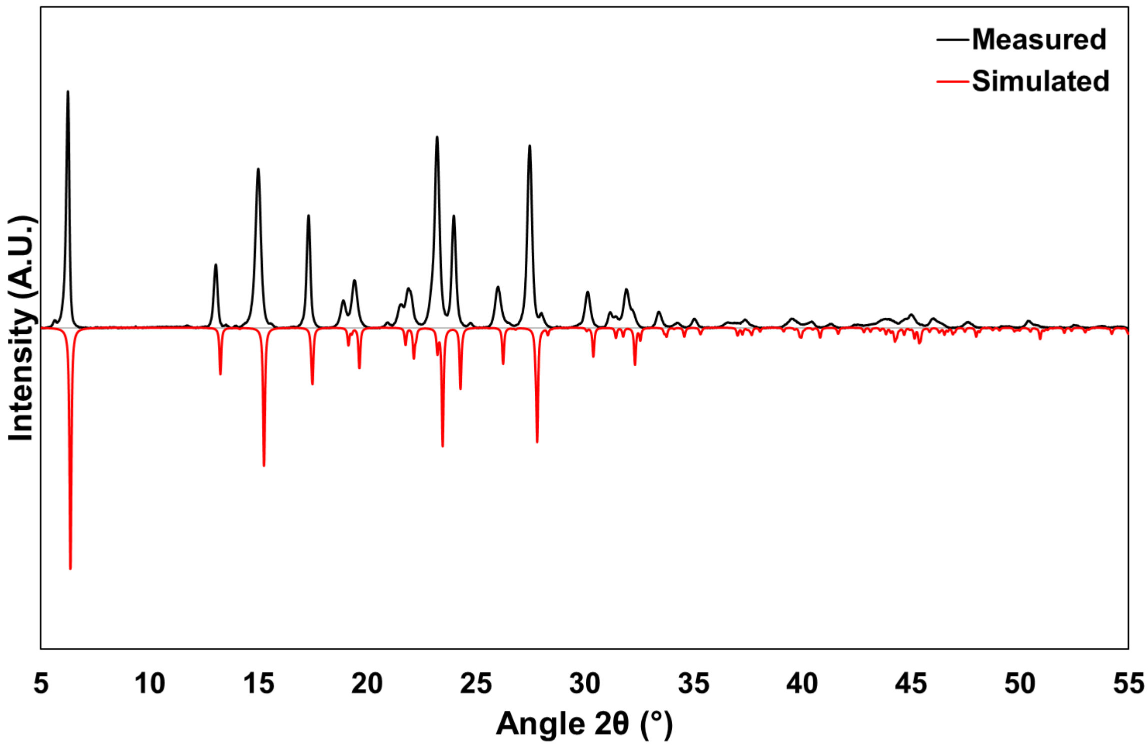

Figure S16 X-ray powder diffraction pattern for complex **2**, showing measured data (black, room temperature) and pattern simulated from single crystal data at 150 K (red)

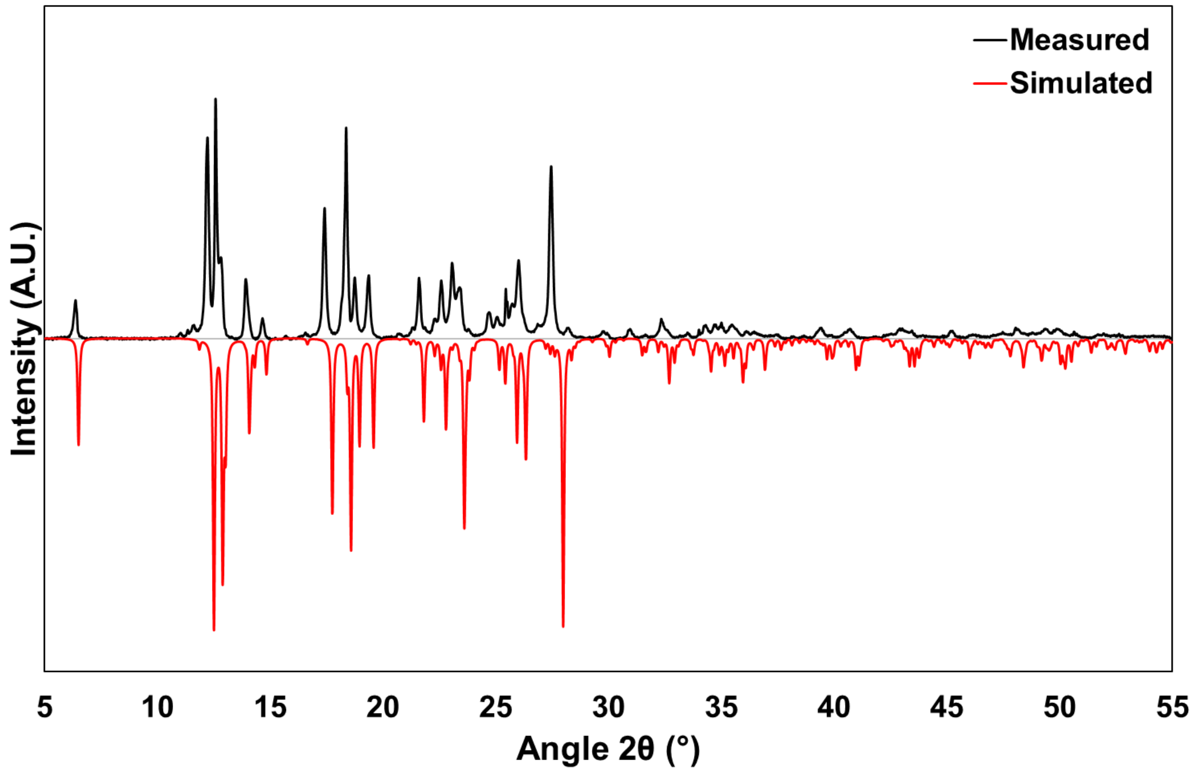

Figure S17 X-ray powder diffraction pattern for complex **3**, showing measured data (black, room temperature) and pattern simulated from single crystal data at 150 K (red)

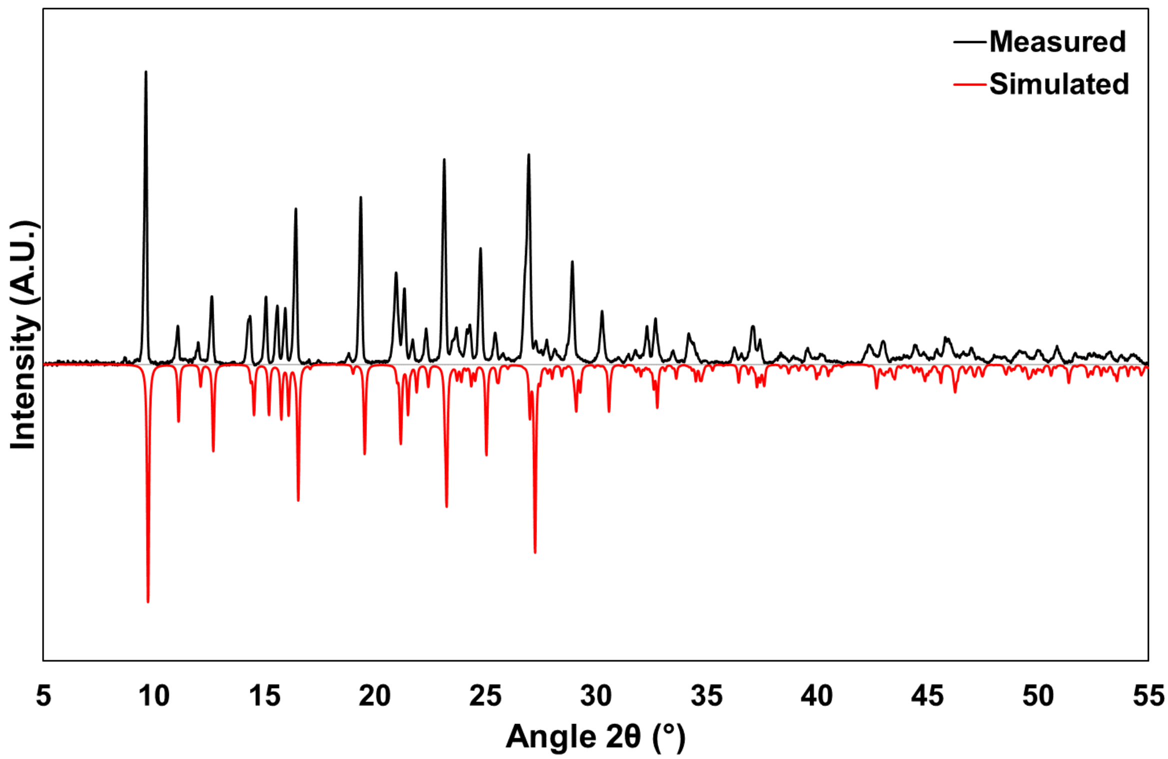

Figure S18 X-ray powder diffraction pattern for complex **3**, showing measured data (black, room temperature) and pattern simulated from single crystal data at 150 K (red)

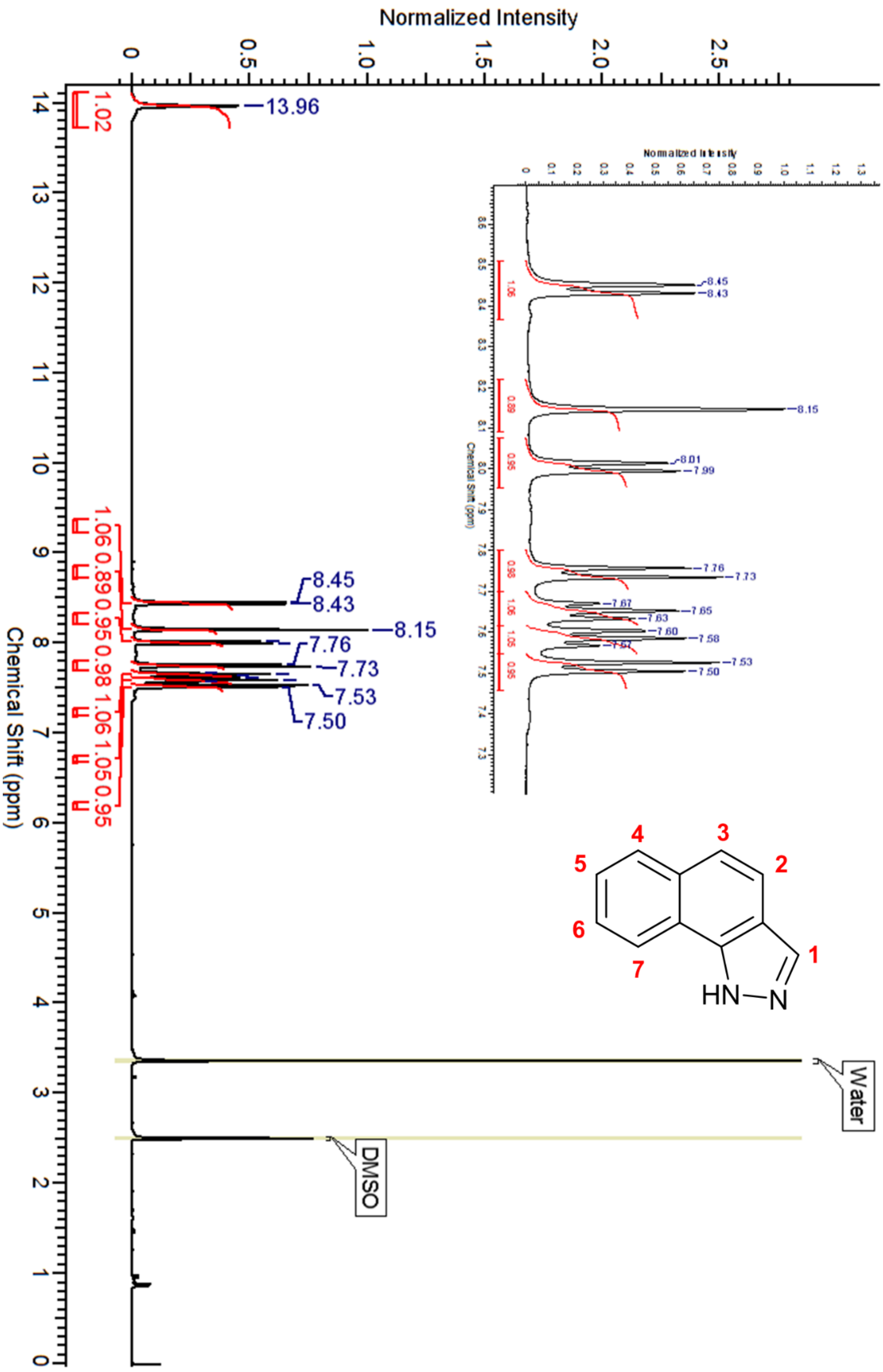

Figure S19 ^{1}H NMR spectrum for **HL1** (d_6-DMSO, 400 MHz), with proton numbering scheme

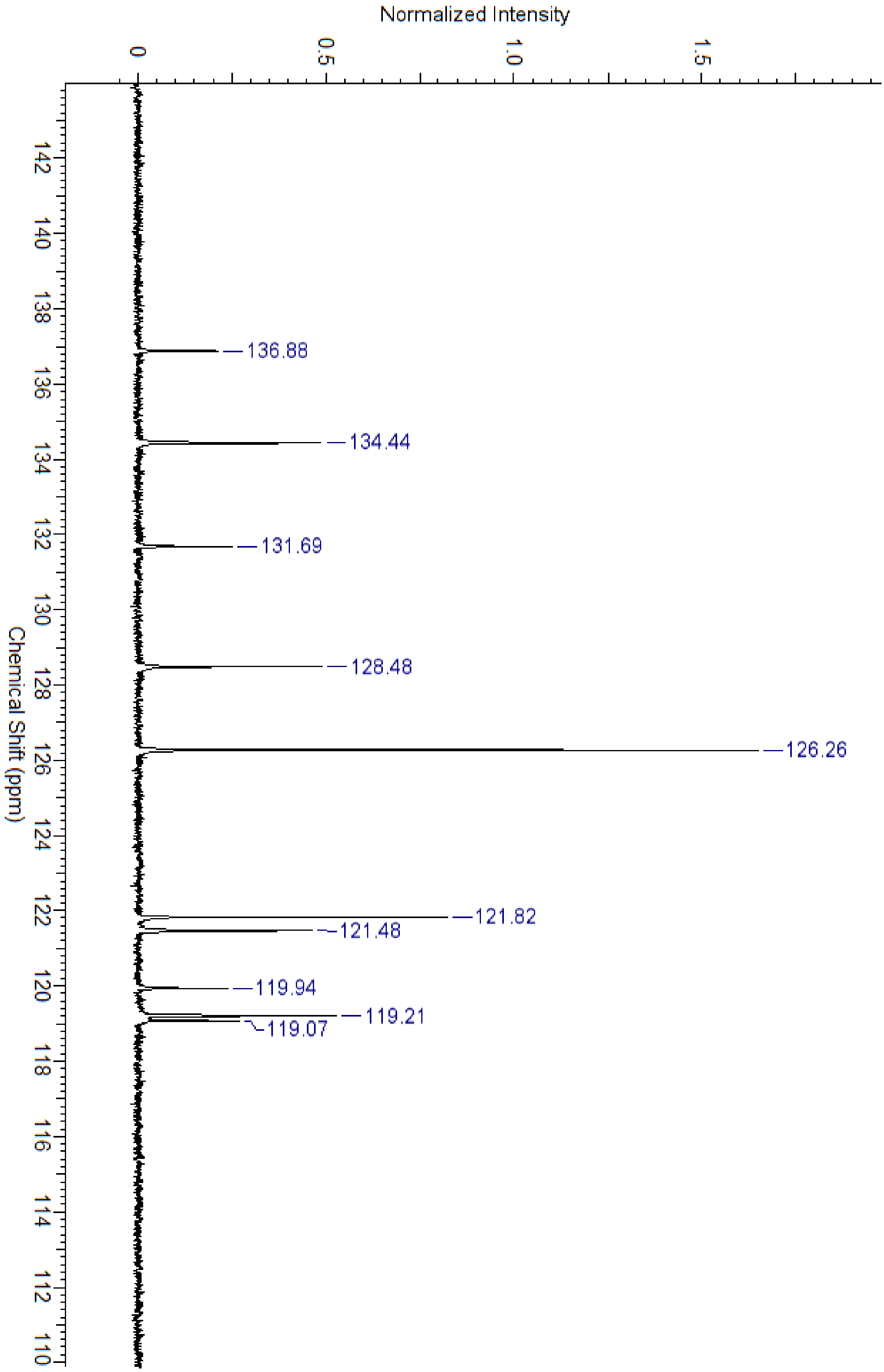

Figure S20 ^{13}C NMR spectrum for **HL1** (d_6-DMSO, 100 MHz)

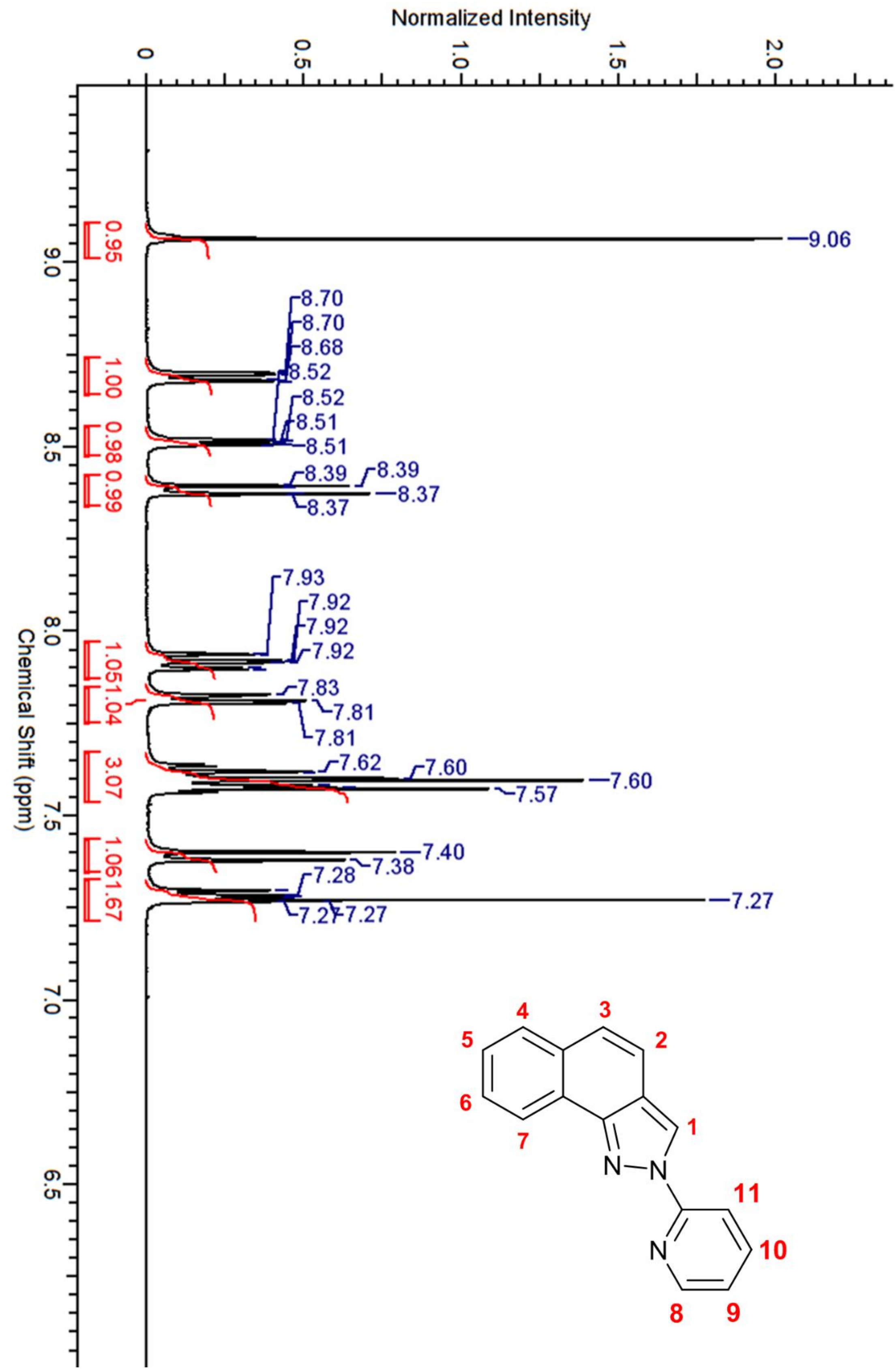

Figure S21 ^{1}H NMR spectrum for **L2** ($CDCl_3$, 400 MHz) with proton numbering scheme

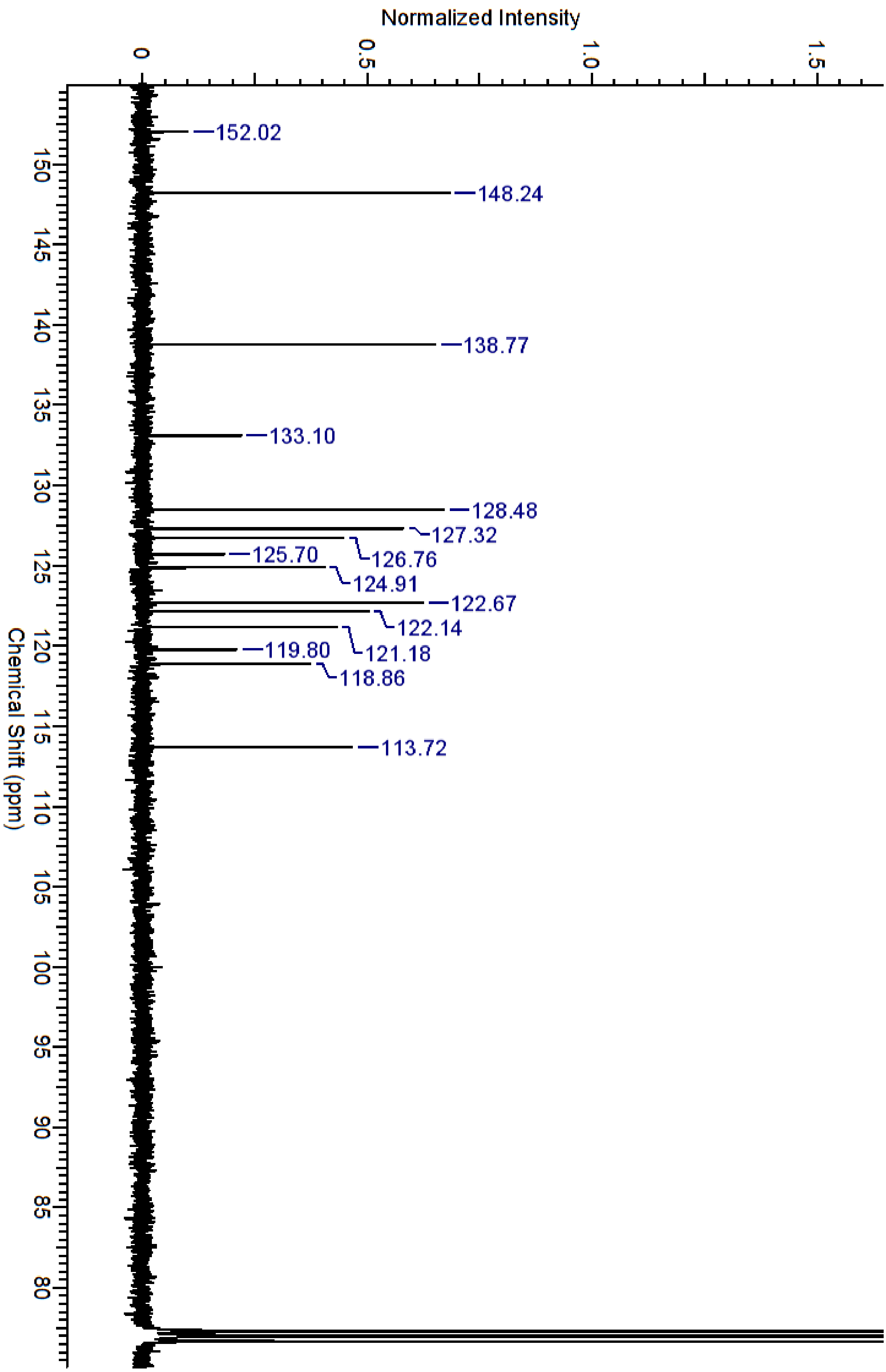

Figure S22 ^{13}C NMR spectrum for **L2** ($CDCl_3$, 100 MHz)